Bone-enhancing microtomography for preclinical imaging

Seung Ho Kim [a], Ho Kyung Kim [a,b*]
[a]*School of Mechanical Engineering, Pusan National University, Busan, South Korea*
[b]*Center for Advanced Medical Engineering Research, Pusan National University, Busan, South Korea*
[*]*Corresponding author: hokyung@pusan.ac.kr*

1. Introduction

We previously described the multilayer ("sandwich") detector by stacking two flat-panel detectors (FPDs) and demonstrated its prospect for "motion-artifact-free" single-shot dual-energy imaging (DEI) by obtaining bone and soft-tissue images of a postmortem mouse [1,2]. While the front FPD measures relatively low energy, the rear one measures relatively high energy because of x-ray beam hardening through the front FPD. Onto the same CMOS photodiode platform, thus, we placed a thicker scintillator in the rear FPD than the front one to achieve high quantum efficiency with the relatively higher-energy x-ray spectrum. An intermediate copper (Cu) filter can be used to further increase spectral separation between the two FPD measurements, which may provide a better contrast-to-noise performance in the subtracted images.

As shown in Fig. 1, the conventional dual-shot image obtained by switching the applied tube voltages (40/70 kVp) showed superior signal-to-noise ratio (SNR) performance but the single-shot image obtained from the sandwich detector was almost as good and had the advantage of being less susceptible to motion artifacts. We also observed that the single-shot method showed better SNR at higher spatial frequencies (e.g. edge regions and bone details) than the double-shot method. The reason can be explained by the inherent "unsharp masking" effect of the sandwich detector; [2] the rear FPD with a thicker scintillator provides a blurrier image than the front FPD, hence subtraction of the two images enhances edges in the resultant image. Inspired by this observation, we have applied the sandwich-detector concept to the microtomography (or micro-CT) for small-animal "bone" imaging.

2. Material and Methods

As shown in Fig. 2, we have developed a bench-top micro-CT system with the sandwich detector. During continuous x-ray irradiation, the object rotates on its axis by an amount of prescribed step angle and then the rotation stays until the sandwich detector produces two projection images. These motion and image readout were computer-controlled and lasted till a single rotation completed. The distances from the x-ray focal spot to the detector (SDD) and to the axis of rotation (SAD) were computer-controlled variables.

The x-ray source (Series 5000 XTF5011, Oxford Instruments, Inc., US) employed a tungsten anode and could operate up to the maximum power of 50 Watts. The tungsten x-ray spectra were further tailored by an additional 1-mm thick aluminum filter. According to the manufacturer, the nominal focal-spot size was 0.035 mm.

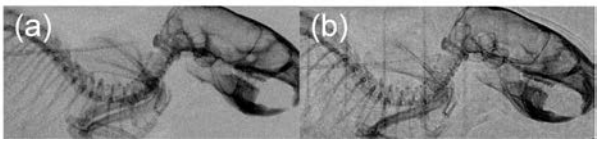

Figure 1. Comparison of dual-energy postmortem mouse images obtained from (a) dual-shot (40/70 kVp switching) and (b) single-shot (using the sandwich detector at 70 kVp) methods

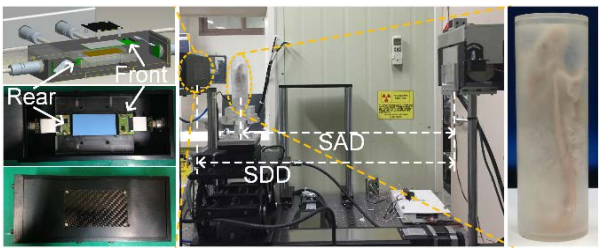

Figure 2. A picture describing the micro-CT system. The enlarged views show the sandwich detector and a postmortem mouse phantom.

Each FPD layer constituting the sandwich detector employed a combination of a Gd_2O_2S:Tb phosphor screen for conversion of x-ray into optical quanta and a photodiode array for detection of them. The thicknesses of the front and rear phosphors were ~ 34 and ~ 67 mg cm^{-2}, respectively. The same photodiode arrays (RadEye1™, Teledyne Rad-icon Imaging Corp., Sunnyvale, US) were used for the front and rear FPDs. The pixel pitch of the photodiode array was 0.048 mm. The active area of the sandwich detector was ~25×50 mm^2. For a small-animal imaging, we prepared a postmortem mouse phantom (~40 g) by replacing blood by paraformaldehyde as shown in Fig. 2. Bone-enhanced tomographic images may be obtained by reconstructing bone-enhanced projection data

$$f_{\text{bone}}(r) = \boldsymbol{FBP}\{\mathbf{W}\mathbf{P}_F - \mathbf{P}_R\}, \quad (1)$$

where $\mathbf{P}_j$ denotes the projection data in a matrix form obtained from the jth FPD layer and $\mathbf{W}$ is a diagonal matrix consisting of weighting factors determined at each projection angle $w(\theta)$. The operator $\boldsymbol{FBP}\{\cdots\}$ implies the approximate filtered backprojection operation [3] and we used the FDK algorithm with the Hann filter. The $w(\theta)$ was determined by minimizing contrast between the soft tissue to be subtracted and background [2]. Head part of a mouse was scanned using two different designs of sandwich detector; one design used no intermediate filter and the other used a Cu filter with a thickness of 0.3 mm. Irradiation x-ray spectrum

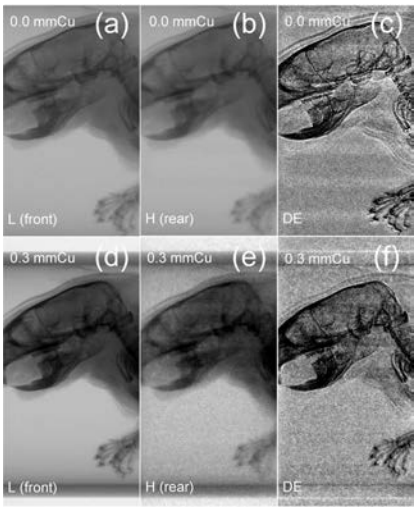

Figure 3. Projection images obtained from the each FPD layer of the sandwich detectors without and with a Cu filter layer and their resultant DE images for the postmortem mouse phantom.

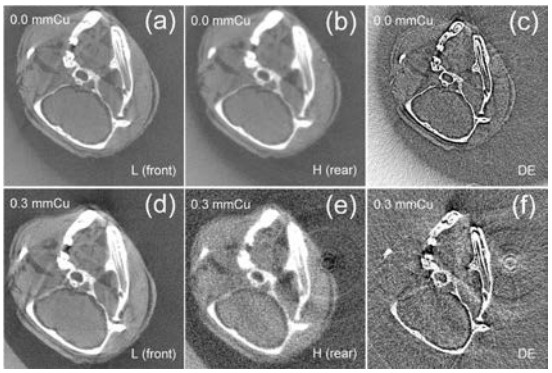

Figure 4. Comparison of tomographic images reconstructed from the corresponding projection dataset.

was from a tungsten target at 50 kVp/1 mm aluminum filter. 360 projection views were obtained for a single circular scan and they were used for reconstruction

3. Preliminary results

Figure 3 compares projection images obtained from the each FPD layer of the two designs of sandwich detectors (i.e. one design included a 0.3 mm-thick Cu filter and the other did not) and their resultant DE images for the postmortem mouse phantom. The images were displayed with the level of their mean value (μ) and a window of two times their standard deviation (σ) (other images below were displayed with the same level and window). It was observed that the projections from the front FPD were sharper than those from the rear FPD as the font FPD employed a thinner phosphor than the rear FPD. Comparing Figs. 3(b) with (e), use of the intermediate filter resulted in higher noise in the rear FPD image, and the reason could be explained by the reduction in the number of x-ray photons reaching the rear FPD due to the attenuation through the filter layer. Weighted logarithmic subtraction successfully provided bone-enhanced images as shown in Figs. 3(c) and (f). Tomographic images reconstructed using each projection dataset, as exemplary shown in Fig. 3, are summarized in Fig. 4. The characteristics observed from the projection data were well reflected into the tomographic images. Comparing Figs. 4(c) with (f), use of the intermediate filter gave rise to a more reduction of soft tissues. It was also observed that the DE tomographic images showed less streak artifacts due to photon starvation compared to the images obtained using the front FPD.

4. Conclusions

Bone-enhanced tomographic images have been obtained using dual-energy sandwich detectors for a postmortem mouse phantom, and they outperformed the tomographic images obtained from the conventional detectors (i.e. the front and rear flat-panel detectors constituting the sandwich detectors) for bone details. Although use of an intermediate filter, which was placed between the front and rear flat-panel detectors, resulted in less residual soft tissues in the reconstructed bone-enhanced images, it degraded the visual image quality of bone details because of increased noise. Optimal filter design in terms of material and thickness is required for a more tissue separability and less noise performance in images.

ACKNOWLEDGMENTS

"This work was supported by the National Research Foundation of Korea (NRF) grant funded by the Korea government (MSIP) (No. 2013M2A2A9046313 and No. 2014R1A2A2A01004416)."

REFERENCES

[1] S. Yun, J. C. Han, D. W. Kim, H. Youn, H. K. Kim, J. Tanguay, and I. A. Cunningham, "Feasibility of active sandwich detectors for single-shot dual-energy imaging," 2014.

[2] J. C. Han, H. K. Kim, D. W. Kim, S. Yun, H. Youn, S. Kam, J. Tanguay, and I. A. Cunningham, "Single-shot dual-energy x-ray imaging with a flat-panel sandwich detector for preclinical imaging," *Current Applied Physics* **14**(12), pp. 1734–1742, 2014.

[3] L. A. Feldkamp, L. C. Davis, and J. W. Kress, "Practical cone-beam algorithm," *J. Opt. Soc. Am. A* **1**, pp. 612–619, Jun 1984.